Benzyltrimethylammonium cadmium dicyanamide with polar order in multiple phases and prospects for linear and nonlinear optical temperature sensing

Mirosław Mączka,*[,a] Anna Gągor,[a] Jan. K. Zaręba.[b] Monika Trzebiatowska,[a] Dagmara Stefańska,[a] Edyta Kucharska,[c] Jerzy Hanuza[a], Norbert Pałka,[d] Elżbieta Czerwińska[d] and Adam Sieradzki[e]

[a]*Institute of Low Temperature and Structure Research, Polish Academy of Sciences, Okólna 2, 50-422 Wrocław, Poland*

[b]*Advanced Materials Engineering and Modeling Group, Wroclaw University of Science and Technology, Wybrzeże Wyspiańskiego 27, 50-370, Wrocław, Poland*

[c]*Department of Bioorganic Chemistry, Faculty of Production Engineering, University of Economics and Business, 118/120 Komandorska str., 53-345 Wrocław, Poland*

[d]*Institute of Optoelectronics, Military University of Technology, S. Kaliskiego 2, 00-908 Warsaw, Poland*

[e]*Department of Experimental Physics, Wrocław University of Science and Technology, Wybrzeże Wyspiańskiego 27, 50-370, Wrocław, Poland*

Table S1. Comparison of the thermometric performance of representative compounds from CPs, QDs (quantum dots), NPs (nanoparticles), and P (microparticles); S_m denotes the highest relative sensitivity at the temperature T_m.

Compound		**T range (K)**	**S_m (%K^{-1})**	**T_m (K)**	**Ref.**
BeTriMeCd		80 – 350[a] 211 – 267[b] 269 – 380[b]	2.59 0.34 0.44	90 239 324	This work
$Eu_{0.0069}Tb_{0.9931}$-DMBDC	CPs	50 - 200	1.15	200	1
$[(Tb_{0.914}Eu_{0.086})_2(PDA)_3(H_2O)]\cdot 2H_2O$		10 - 325	5.96	25	2
$Tb_{0.99}Eu_{0.01}(BDC)_{1.5}(H_2O)_2$		290 - 320	0.31	318	3
$Gd_{0.7638}Tb_{0.2188}Eu_{0.0174}$(phen)(1,3,5-btc)(DMF)·DMF		293 - 393	2.71[c] 2.91[d]	All range	4
$Tb_{0.8}Eu_{0.2}$(bpda)		293 - 328	1.19	313	5
$[Me_2NH_2][Eu_{0.0066}Tb_{0.9934}(ddcpp)(H_2O)_2]$		77 - 450	3.76	450	6
$(Me_2NH_2)_3[Eu_3(FDC)_4(NO_3)_4]_4H_2O$		12 - 320	2.70	170	7
$Sr(HCOO)_2$:Eu^{2+}/Eu^{3+}		9 - 293	3.80	293	8
$Tb_{0.995}Eu_{0.005}$@In(OH)(bpydc)		283-333	4.97	-	9
$Tb_{0.8}Eu_{0.2}$(bpda)		298-318	1.19	313	10
$[Me_2NH_2][Eu_{0.0066}Tb_{0.9934}(ddcpp)(H_2O)_2]$		77-450	3.76	450	11
$Tb_{0.95}Eu_{0.05}$HL		4-50	31	4	12
$[Eu_{0.102}Tb_{0.898}(notpH_4)(NO_3)(H_2O)]_8H_2O$		18 - 300	3.90	38	13
$Tb_{0.957}Eu_{0.043}$cpda		40 - 300	1.77	250	14
$Tb_{0.9}Eu_{0.1}(PIA)(HPIA)(H_2O)_{2.5}$		100 - 300	3.26	300	15
$Tb_{0.99}Eu_{0.01}(bdc)_{1.5}\cdot(H_2O)_2$		290 - 320	0.30	310	16
$[Tb(H_5btp)]\cdot 2H_2O$		299 - 319	1.43	310	17

CdSe	QDs	82 - 280	0.69	200	18
CdTe		80 - 360	0.7	199	19
CdSe/ZnS		278 - 313	0.025	313	20
$Zn_{1-x}Mn_xSe/ZnCdSe$		134 - 400	0.07	134	21
SrF_2:Yb, Er	NPs	298 - 383	1.21	298	22
$(Gd_{0.98}Nd_{0.2})_2O_3$		298 - 338	2.18	298	23
$YVO_4:Nd^{3+}$		123 - 873	1.50	283	24
$NaYF_4:Nd^{3+}$		273 - 423	0.12	273	25
$Ba_2MgWO_6:Eu^{3+}$	P	80 - 375	1.5	120	26
$Sr_2(Ge, Si)O_4$: Pr^{3+}		20 - 700	2.94	225	27
$Ca_2Mg_{0.5}AlSi_{1.5}O_7:Eu^{2+}$		80 - 575	1.62	350	28
$La_{0.4}Gd_{1.6}Zr_2O_7:Pr^{3+}$		15 - 650	0.81	650	29
$Mg_2Al_4Si_5O_{18}:Eu^{2+}$		25 - 425	0.45	400	30

a – luminescence thermometry under linear excitation (266 nm)
b – SHG single band thermometry (800 nm pumping)
c – one-photon excitation at 377 nm,
d – three-photon excitation at 800 nm

1. Y. Cui, H. Xu, Y. Yue, Z. Guo, J. Yu, Z. Chen, J. Gao, Y. Yang, G. Qian and B. Chen, *J. Am. Chem. Soc.*, 2012, **134**, 3979–3982.
2. Z. Wang, D. Ananias, A. Carné-Sánchez, C. D. S. Brites, I. Imaz, D. Maspoch, J. Rocha and L. D. Carlos, *Adv. Funct. Mater.*, 2015, **25**, 2824–2830.
3. A. Cadiau, C. D. S. Brites, P. M. F. J. Costa, R. A. S. Ferreira, J. Rocha and L. D. Carlos, *ACS Nano*, 2013, **7**, 7213–7218.
4. J. K. Zaręba, M. Nyk, J. Janczak, and M. Samoć, *ACS Appl. Mater. Interfaces* 2019, **11**, 10435–10441.
5. D. Zhao, X. Rao, J. Yu, Y. Cui, Y. Yang and G. Qian, *Inorg. Chem.*, 2015, **54,** 11193-11199.
6. Y. Yang, L. Chen, F. Jiang, M. Yu, X. Wan, B. Zhang and M. Hong, *J. Mat. Chem. C*, 2017, **5,** 1981-1989.
7. L. Li, Y. Zhu, X. Zhou, C. D. S. Brites, D. Ananias, Z. Lin, F. A. A. Paz, J. Rocha, W. Huang and L. D. Carlos, *Adv. Funct. Mater.*, 2016, **26**, 8677–8684.
8. W. Liu, L. Liu, Y. Wang, L. Chen, J. A. McLeod, L. Yang, J. Zhao, Z. Liu, J. Diwu, Z. Chai, T. E. Albrecht-Schmitt, G. Liu and S. Wang, *Chem. - A Eur. J.*, 2016, **22**, 11170–11175.
9. Y. Zhou, B. Yan and F. Lei, *Chem. Commun.*, 2014, **50**, 15235–15238.
10. D. Zhao, X. Rao, J. Yu, Y. Cui, Y. Yang and G. Qian, *Inorg. Chem.*, 2015, **54**, 11193–11199.
11. Y. Yang, L. Chen, F. Jiang, M. Yu, X. Wan, B. Zhang and M. Hong, *J. Mater. Chem. C*, 2017, **5**, 1981–1989.
12. X. Liu, S. Akerboom, M. De Jong, I. Mutikainen, S. Tanase, A. Meijerink and E. Bouwman, *Inorg. Chem.*, 2015, **54**, 11323–11329.
13. M. Ren, C. D. S. Brites, S.-S. Bao,Rute A. S. Ferreira, L.-M. Zheng and L. D. Carlos *J. Mater. Chem. C*, 2015, **3**, 8480—8484.
14. Y. J. Cui, W. F. Zou, R. J. Song, J. C. Yu, W. Q. Zhang, Y. Yangand G. D. Qian, *Chem. Commun.*, 2014, **50**,

719.
15. X. Rao, T. Song, J. Gao, Y. Cui, Y. Yang, C. Wu, B. Chen and G. Qian, *J. Am. Chem. Soc.*, 2013, **135**, 15559-15564.
16. A. Cadiau, C. D. S Brites, P. Costa, R. A. S. Ferreira, J. Rocha, L. D. Carlos, Ratiometric Nanothermometer Based on an Emissive Ln^{3+}-Organic Framework ACS Nano 2013, **7**, 7213– 7218
17. D. Ananias, A. D. G. Firmino, R. F. Mendes, F. A. A. Paz, M. Nolasco, L. D. Carlos, and J. Rocha, *Chem. Mater.*, 2017, **29**, 9547–9554.
18. L. Jethi, M. M. Krause and P. Kambhampati, *J. Phys. Chem. Lett.*, 2015, **6**, 718–721.
19. S. Kalytchuk, O. Zhovtiuk, S. V. Kershaw, R. Zbořil and A. L. Rogach, *Small*, 2016, **12**, 466–476.
20. G. W. Walker, V. C. Sundar, C. M. Rudzinski, A. W. Wun, M. G. Bawendi and D. G. Nocera, *Appl. Phys. Lett.*, 2003, **83**, 3555–3557.
21. V. A. Vlaskin, N. Janssen, J. Van Rijssel, R. Beaulac and D. R. Gamelin, *Nano Lett.*, 2010, **10**, 3670–3674.
22 S. Balabhadra, M. L. Debasu, C. D. S. Brites, R. A. S. Ferreira and L. D. Carlos, *J. Phys. Chem. C*, 2017, **121**, 13962–13968.
23. M. L. Debasu, H. Oliveira, J. Rocha and L. D. Carlos, *J. Rare Earths*, 2020, **38**, 483–491.
24. A. A. Kalinichev, M. A. Kurochkin, E. V. Golyeva, A. V. Kurochkin, E. Lähderanta, M. D. Mikhailov and I. E. Kolesnikov, *J. Lumin.*, 2018, **195**, 61–66.
25. D. Wawrzynczyk, A. Bednarkiewicz, M. Nyk, W. Strek and M. Samoc, *Nanoscale*, 2012, **4**, 6959–6961.
26. D. Stefańska, B. Bondzior, T. H. Q. Vu, N. Miniajluk-Gaweł and P. J. Dereń, *J. Alloys Compd.*, 2020, **842**, 155742.
27. M. Sójka, J. F. C. B. Ramalho, C. D. S. Brites, K. Fiaczyk, L. D. Carlos and E. Zych, *Adv. Opt. Mater.*, 2019, **7**, 1901102.
28. D. Stefańska, M. Stefanski and P. J. Dereń, *J. Alloys Compd.*, 2021, **863**, 158770.
29. J. Trojan-Piegza, C. D. S. Brites, J. F. C. B. Ramalho, Z. Wang, G. Zhou, S. Wang, L. D. Carlos and E. Zych, *J. Mater. Chem. C*, 2020, **8**, 7005–7011.
30. D. Stefańska and P. J. Dereń, *Adv. Opt. Mater.*, 2020, **18**, 2001143.

Table S2. Experimental details

For all structures: $C_{16}H_{16}CdN_{10}$, M_r = 460.79.

	Phase I	**Phase II**
Crystal data		
Crystal system, space group	Orthorhombic, $Cmc2_1$	Monoclinic, $P2_1$
Temperature (K)	295	120
a, b, c (Å)	9.9628 (5), 14.1773 (6), 14.0487 (4)	8.1130 (6), 14.0621 (6), 8.9405 (3)
α, β, γ (°)	90, 90, 90	90, 110.376 (4), 90
V (Å^3)	1984.32 (14)	956.16 (9)
Z	4	2
μ (mm^{-1})	1.12	1.17
Crystal size (mm)	0.19 × 0.15 × 0.10	0.19 × 0.15 × 0.10
Data collection		
T_{min}, T_{max}	0.871, 1.000	0.993, 1.000
No. of measured, independent and observed [$I > 2\sigma(I)$] reflections	14992, 2688, 2034	8299, 8299, 7517
R_{int}	0.022	0.035
$(\sin \theta/\lambda)_{max}$ (Å^{-1})	0.692	0.823
Refinement		
$R[F^2 > 2\sigma(F^2)]$, $wR(F^2)$, S	0.027, 0.058, 1.02	0.053, 0.153, 1.08
No. of reflections	2688	8299
No. of parameters	155	247
No. of restraints	8	9
H-atom treatment	H-atom parameters constrained	H-atom parameters constrained
$\Delta\rangle_{max}$, $\Delta\rangle_{min}$ (e Å^{-3})	0.14, -0.26	1.38, -2.27
Absolute structure	Flack x determined using 806 quotients [(I+)-(I-)]/[(I+)+(I-)] (Parsons, Flack and Wagner, Acta Cryst. B69 (2013) 249-259).	Refinement based on two twin components with hklf 5.
Absolute structure parameter	-0.033 (11)	-

Computer programs: *CrysAlis PRO* 1.171.38.41 (Rigaku OD, 2015), *CrysAlis PRO* 1.171.38.46 (Rigaku OD, 2015), *SHELXT* 2014/5 (Sheldrick, 2014), *SHELXL2018*/3 (Sheldrick, 2018).

Table S3. Selected geometric parameters (Å, º)

295 K			
Cd1—N4	2.305 (4)	Cd1—N1	2.332 (6)
Cd1—N4^{i}	2.305 (4)	Cd1—N6^{iii}	2.341 (4)
Cd1—N3^{ii}	2.328 (5)	Cd1—N6^{iv}	2.341 (4)
N4—Cd1—N4^{i}	87.5 (2)	N3^{ii}—Cd1—N6^{iii}	89.35 (13)
N4—Cd1—N3^{ii}	88.40 (13)	N1—Cd1—N6^{iii}	82.1 (3)
N4^{i}—Cd1—N3^{ii}	88.40 (13)	N4—Cd1—N6^{iv}	91.81 (14)
N4—Cd1—N1	100.1 (2)	N4^{i}—Cd1—N6^{iv}	177.67 (13)
N4^{i}—Cd1—N1	89.5 (3)	N3^{ii}—Cd1—N6^{iv}	89.35 (12)
N3^{ii}—Cd1—N1	171.1 (3)	N1—Cd1—N6^{iv}	92.8 (3)
N4—Cd1—N6^{iii}	177.67 (13)	N6^{iii}—Cd1—N6^{iv}	88.8 (2)
N4^{i}—Cd1—N6^{iii}	91.81 (15)		
120 K			
Cd1—N1	2.279 (8)	Cd1—N6^{vi}	2.611 (9)
Cd1—N3^{v}	2.202 (8)	Cd1—N7	2.221 (8)
Cd1—N4	2.662 (10)	Cd1—N9^{v}	2.218 (8)
N1—Cd1—N4	79.1 (3)	N7—Cd1—N1	73.0 (3)
N1—Cd1—N6^{vi}	97.6 (3)	N7—Cd1—N4	84.2 (3)
N3^{v}—Cd1—N1	175.0 (3)	N7—Cd1—N6^{vi}	94.5 (3)
N3^{v}—Cd1—N4	96.8 (3)	N9^{v}—Cd1—N1	109.3 (3)
N3^{v}—Cd1—N6^{vi}	86.4 (3)	N9^{v}—Cd1—N4	94.5 (3)
N3^{v}—Cd1—N7	103.9 (3)	N9^{v}—Cd1—N6^{vi}	86.9 (3)
N3^{v}—Cd1—N9^{v}	73.8 (3)	N9^{v}—Cd1—N7	177.2 (3)
N6^{vi}—Cd1—N4	176.7 (3)		

Symmetry code(s): (i) -*x*+1, *y*, *z*; (ii) -*x*+1, -*y*+1, *z*-1/2; (iii) -*x*+1, -*y*+1, *z*+1/2; (iv) *x*, -*y*+1, *z*+1/2; (v) -*x*, *y*-1/2, -*z*+1; (vi) -*x*, *y*+1/2, -*z*+1.

Table S4. Selected hydrogen-bond parameters at 120 K with atom numbering, below.

D—H···*A*	*D*—H (Å)	H···*A* (Å)	*D*···*A* (Å)	*D*—H···*A* (°)
C5—H5A···N4^{iv}	0.97	2.19	2.927 (12)	135.7
C7—H7A···N1	0.97	2.09	3.063 (12)	177.1
C7—H7B···N7^{i}	0.97	2.45	3.402 (12)	167.6
C8—H8A···N3^{ii}	0.96	2.43	2.901 (12)	110.3
C8—H8C···N9^{iii}	0.96	2.02	2.890 (12)	150.1
C9—H9A···N6^{iv}	0.96	2.19	3.040 (12)	147.3
C10—H10A···N6^{v}	0.96	2.34	3.210 (12)	150.3

Symmetry code(s): (i) *x*+1, *y*, *z*; (ii) -*x*+1, *y*-1/2, -*z*+1; (iii) -*x*, *y*-1/2, -*z*+1; (iv) -*x*+1, *y*+1/2, -*z*+1; (v) -*x*, *y*+1/2, -*z*+1.

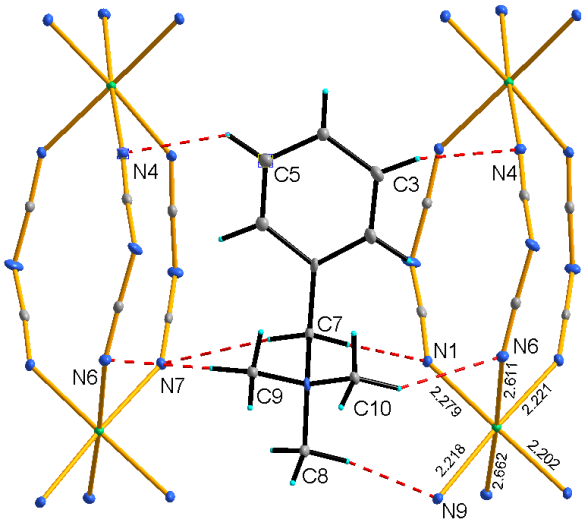

Table S5. Raman wavenumbers (in cm-1) of BeTriMeCd at 80, 270, 380 K (heating) and 80 K (cooling back).a Bold numbers correspond to the RT Raman bands observed in the spectra measured using the eclipse filter.

80 K	270 K	380 K	80 K- cooling back	Assignment
3068sh+3063m	3071m+3065m	3070m	3067m	νCH
			3047vw	νCH
3049w+3044sh	3050w+3040m	3036m	3035sh+3032m	$\nu_{as}CH_3$
+3040m 3030m	3030m+3021w	3030m	3025m	$\nu_{as}CH_3$
+3024m+3019w				$\nu_{as}CH_3$
	3013w+3001m	2998vw	3011w+3000w	$\nu_{as}CH_3$
3011w+3003m 2982m	2979m	2977m	2984m	ν_sCH_3+ ν_sCH_2
2969m+2961w+2954w	2966m	2962w	2971w+2961w	ν_sCH_3
2924w+2911w	2918w+2911w	2907vw	2943w	ν_sCH_3
2897w	2896w		2919vw+2909w	overtone
2239vs	2234vs	2232s	2242vs	$\nu_sC{\equiv}N$
2229w			2237s	$\nu_sC{\equiv}N$
2220w			2213s	$\nu_sC{\equiv}N$
2208w	2206vw			$\nu_sC{\equiv}N$
2166w+2155w 2147m	2162w+2152w		2175w	$\nu_{as}C{\equiv}N$
+2140m 1615w	2142m	2150vw	2163w+2136w	$\nu_{as}C{\equiv}N$ overtone
1603m	1615w			νϕ
1585w	1602m	1602m	1603w	νϕ
1491vw	1585w		1584vw	δCH
1479vw+1473vw	1488vw			$\delta_{as}CH_3$
1465m	1474vw	1474vw	1484w+1475w	$\delta_{as}CH_3$
1454m+1440w	1463m	1459w	1460w+1453w	δ_sCH_3
1419w	1451m+1440w	1448m	1447w+1441w	δ_sCH_3
1380w	1418w	1417vw		$\nu_{as}N$-C
1266w	1375m	1373vw	1380w	ρCH_3
1246w	1264w			ρCH_3
1215m	1244w	1238vw	1247w	νϕ-CH_2
1203w+1186w	1213m	1215m	1217w+1200w	ρCH_3
1162w	1201w+1185w	1188vw	1179w	δCH
1123w	1162w	1160w	1156w	ρCH_3
1079w	1122w	1123vw	1125vw	δCH
1059w	1079vw		1089vw	δCH
1030w	1064vw			νϕ
1003m	1030w	1032w	1029w	$\nu_s\phi$
992w+998w	1003m	1003m	1002m	γCH
975w	990w		987w	νN-CH_3
936w	975w		980w	ν_sN-C
926w+923sh	934w	918w	923w	ν_sN-C
891m	921w			νN-CH_3+$\rho CH_2\gamma$
848w	888m	883w	896w	CH
834m	847w			νN-CH_3+νCH_2-N
822vw	834m	835m	835w	ϕδ
779w	818vw		818vw	γCH+νN-CH_3
724m	778w	777w	783w	γ+ϕγCH
702w	722m	723m	730w	ν+ϕγCH_2-N
675m+667m	702w	700w	704w	δ_sN-C-N
620w	675m	655m	651m	ϕδ
	621w	621w	620w	

608vw	609vw	611vw	612vw	$\phi\delta$
551vw+537w	548vw+536w	535w	561w+543w	γ_sN-C-N
527w				γ_{as}N-C-N +$\phi\gamma$
514w	513w	514vw	514w	δ_{as}N-C-N
449w	446w			$\phi\gamma$
414w+396w	416w+393w	420vw	423w+390w	$\phi\gamma$
331vw+321w	315w			τCH3
				τCH3
303w+294w	**300w**		**301w+288w**	$\phi\rho$-CH2-N +τCH3
275m	**275w**	**273w**	**277w**	
254w	**244sh**		**259w+238w**	νCd-N
243w+207m	**214m+204m**	**208sh+178m**	**194sh+184m**	νCd-N+δ_sC-N-C
186w+167w			**168w**	νCd-N
154sh+148w	**143sh**		**155w**	ωCd-N+T'(BeTriMe)
134m+123w	**130m**	**125sh**		ωCd-N+T'(BeTriMe)
111m+100w	**108m**	**107m**	**124w+112m**	ωCd-N+T'(BeTriMe)+$\phi\gamma$-CH_2-N
89sh+83w	**75m**	**79m**	**88m+75m**	ωCd-N+$\phi\gamma$-CH_2-N
57s	**50sh**		**67s**	L(CdN_6)
44s+39s	**40vs**	**38s**	**57s**	L(CdN_6)
29s	**30vs**	**27s**		L(CdN_6)

[a]Key: s, strong; m, medium; w, weak; vw, very weak; sh, shoulder; b, broad; ν, δ, γ, ω, τ, ρ, T' and L denotes stretching, in-plane bending, out-of-plane bending, wagging, twisting, rocking, translational and librational, respectively.

Table S6. RT IR and THz (bold) wavenumbers (in cm^{-1}) of BeTriMeCd as well as ATR IR wavenumbers of the sample heat-treated at 400 K.[a]

300 K	Heat-treated at 400 K	Assignment
3564w	3595w	overtone
3480vw	3568vw	overtone
3221w	3215w	overtone
3060w	3063w + 3051w	νCH
3039w	3034w	$\nu_{as}CH_3$
2295s	2296s	overtone
2233sh		$\nu_s C{\equiv}N$
2223m	2235m	$\nu_s C{\equiv}N$
2203w	2215w	$\nu_s C{\equiv}N$
2160vs	2166sh+2155s+2139s	$\nu_{as} C{\equiv}N$
1601vw		νϕ
1585vw		νϕ
1485w	1486w	δCH
1474m	1474w	$\delta_{as}CH_3$
1462vw	1461vw	$\delta_{as}CH_3$
1456w	1456w	$\delta_s CH_3$
1419w	1417w	$\delta_s CH_3$
1375w	1369s	ν_{as}N-C
1353s	1359s	ν_{as}N-C
1243w	1244w	ρCH_3
1214m	1216m	$\nu\phi$-CH_2
1185w	1186w	ρCH_3
1123w	1125w	ρCH_3
1081w	1080w	$\nu\rho+\phi CH_3$
1067w		δCH
1030w	1034w	νϕ
1004w	1003w	$\nu_s\phi$
988w	987w	γCH
974w	977w	νN-CH_3
927w+921w	919m	ν_sN-C
888m	889m	νN-$CH_3+\rho CH_2$
872sh	875sh	γCH
778w	780w	$\gamma CH+\nu$N-CH_3
723m	726m	$\gamma+\phi\gamma CH$
702m	701m	$\nu+\phi\gamma CH_2$-N
671m+666sh	651m	δ_sN-C-N
610vw	613vw	ϕδ
530m	537sh	γ_sN-C-N
513w	508m	γ_{as}N-C-N +ϕγ
454w	456w	ϕγ
418vw		ϕγ
301vw		τCH_3
291vw		τCH_3
276w		$\phi\rho$-CH_2-N $+\tau CH_3$
239w		νCd-N+δ_sC-N-C
188m		νCd-N
136m		ωCd-N+T'(BeTriMe)
71w		ωCd-N+$\phi\gamma$-CH_2-N
38m		L(CdN_6)+L($BeTriMe^+$)+ϕ
		γ-CH_2-N-CH_3

[a]Key: s, strong; m, medium; w, weak; vw, very weak; sh, shoulder; b, broad; ν, δ, γ, ω, τ, ρ, T' and L denotes stretching, in-plane bending, out-of-plane bending, wagging, twisting, rocking, translational and librational, respectively.

Table S7. Mulliken atomic charges for $BeTriMe^+$. C_B – carbon atoms of the benzene ring, C_B^* – carbon atom of the benzene ring bonded to the CH_2 bridge, C_M – carbon atoms of the methyl CH_3 groups, C_m – carbon atoms of the methylene CH_2 group.

No	Symbol	Charge
1	N	-0.334756
2	C_B^*	-0.006318
3	C_B	-0.100139
4	H	0.076060
5	C_M	-0.035711
6	H	0.110104
7	H	0.117230
8	H	0.123416
9	C_B	-0.041859
10	H	0.089978
11	C_m	0.050514
12	H	0.119373
13	H	0.119493
14	C_B	-0.035694
15	H	0.093887
16	C_B	-0.041758
17	H	0.089944
18	C_M	-0.032012
19	H	0.115982
20	H	0.115971
21	H	0.115671
22	C_B	-0.100444
23	H	0.076084
24	C_M	-0.035791
25	H	0.117301
26	H	0.110174
27	H	0.123297

Table S8. Changes of CIE chromaticity and emission colour of BeTriMeCd with temperature.

Temperature (K)	CIE chromaticity of BeTriMeCd		Colour of emission
	x	y	
80	0.21	0.23	blue
90	0.22	0.25	greenish blue
100	0.24	0.26	greenish blue
110	0.25	0.28	greenish blue
120	0.26	0.29	greenish blue
130	0.27	0.31	bluish green
140	0.29	0.32	bluish green
150	0.30	0.32	white
160	0.31	0.33	white
170	0.31	0.34	white
180	0.32	0.34	white
190	0.33	0.34	white
200	0.34	0.35	white
210	0.35	0.35	white
220	0.36	0.36	white
230	0.37	0.36	white
240	0.37	0.36	white
250	0.38	0.36	white
260	0.38	0.37	white
270	0.39	0.38	greenish yellow
280	0.39	0.39	greenish yellow
290	0.38	0.38	greenish yellow
300	0.38	0.38	greenish yellow
310	0.38	0.39	greenish yellow
320	0.38	0.39	greenish yellow
330	0.38	0.40	greenish yellow
340	0.38	0.41	greenish yellow
350	0.38	0.41	greenish yellow
360	0.39	0.42	greenish yellow
370	0.40	0.42	greenish yellow
380	0.40	0.43	greenish yellow
390	0.39	0.43	greenish yellow
400	0.40	0.43	greenish yellow
410	0.40	0.43	greenish yellow

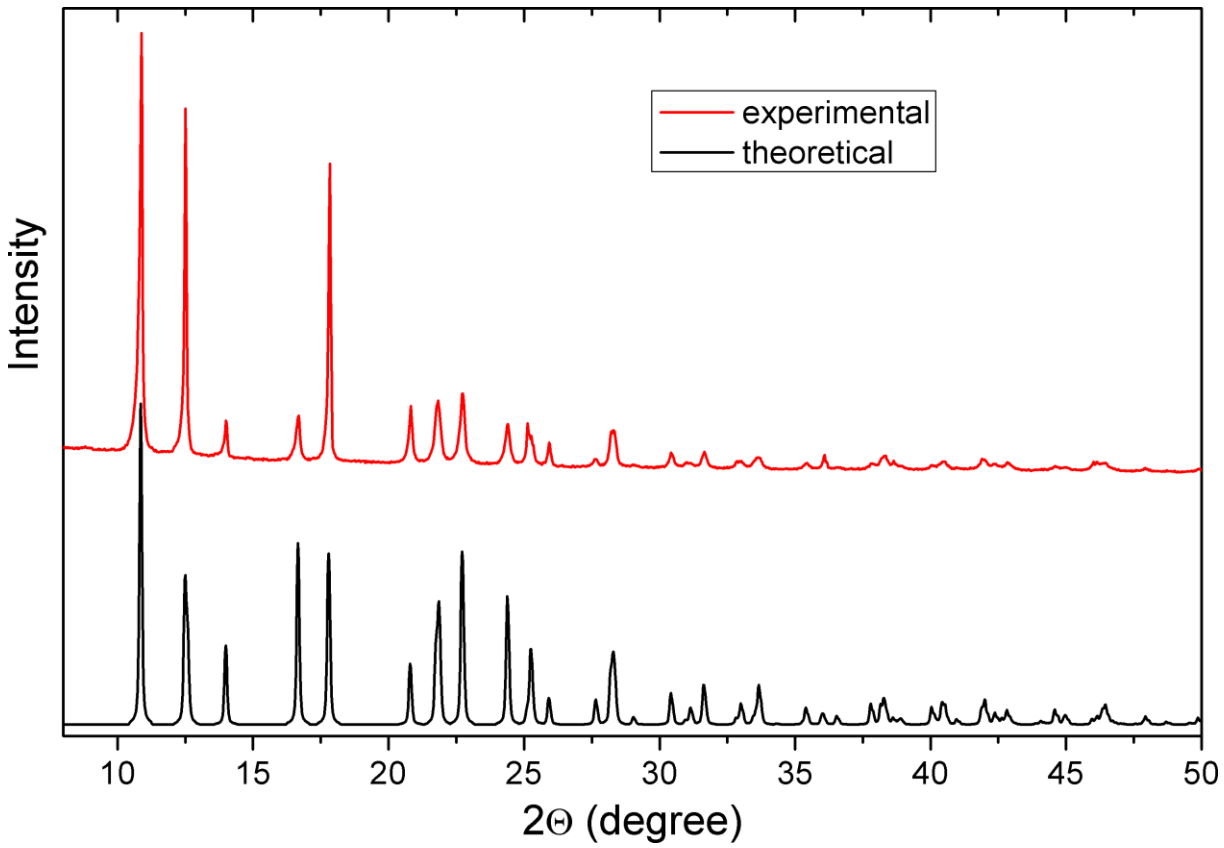

Figure S1. Room-temperature powder XRD pattern for the as-prepared BeTriMeCd together with the calculated one based on the RT single crystal structure.

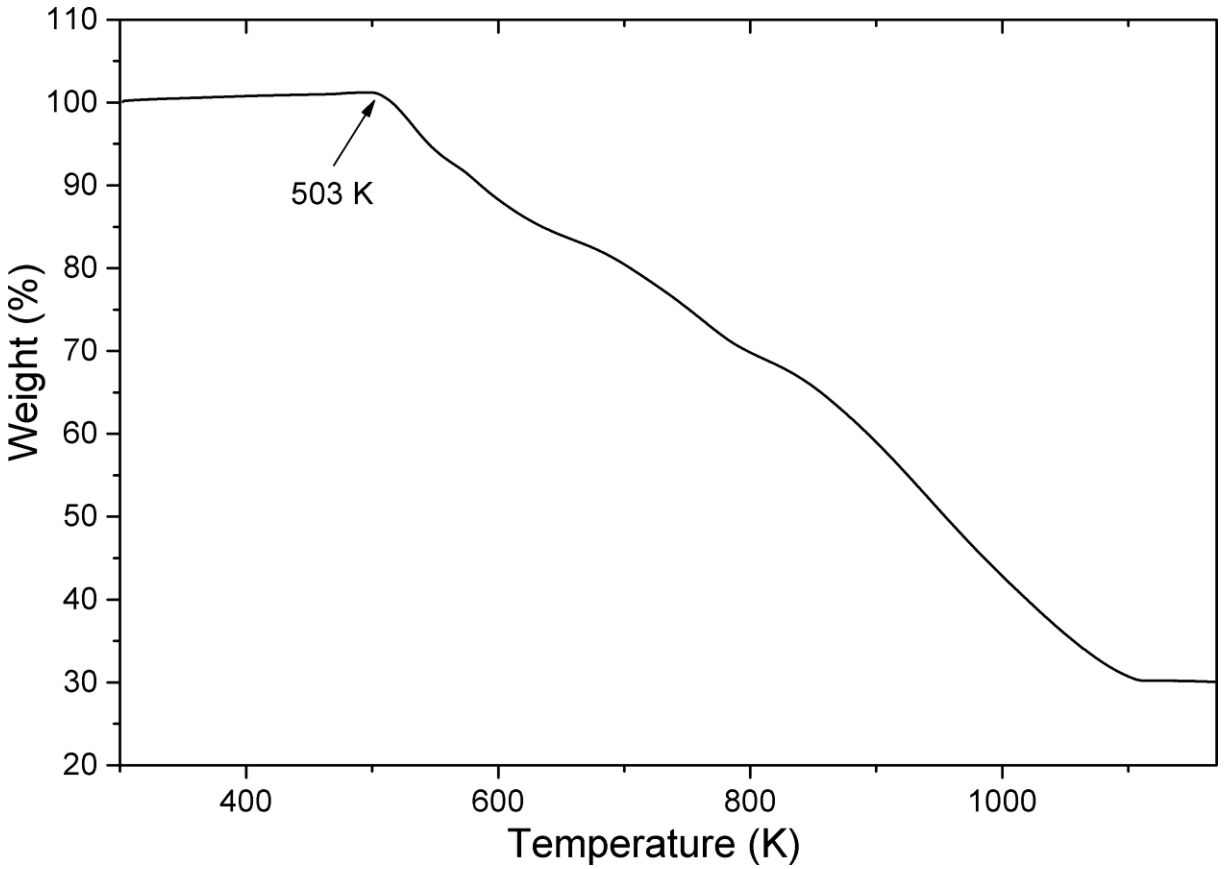

Figure S2. TGA plot of BeTriMeCd.

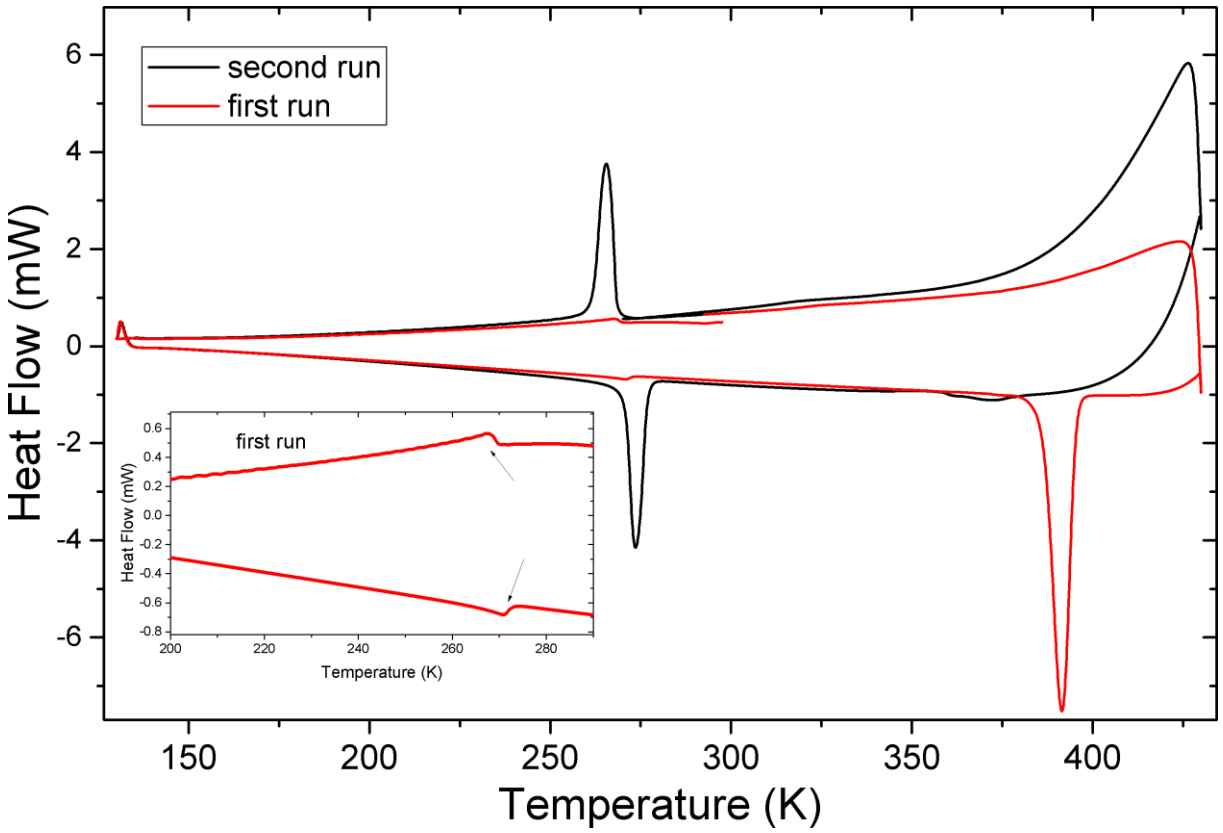

Figure S3. DSC traces for BeTriMeCd: cooling from 298 K to 130 K, heating to 430 K and cooling to 290 K (1st run, red line; 2nd run, black). Insert shows weak DSC anomalies near 270 K observed during the first run.

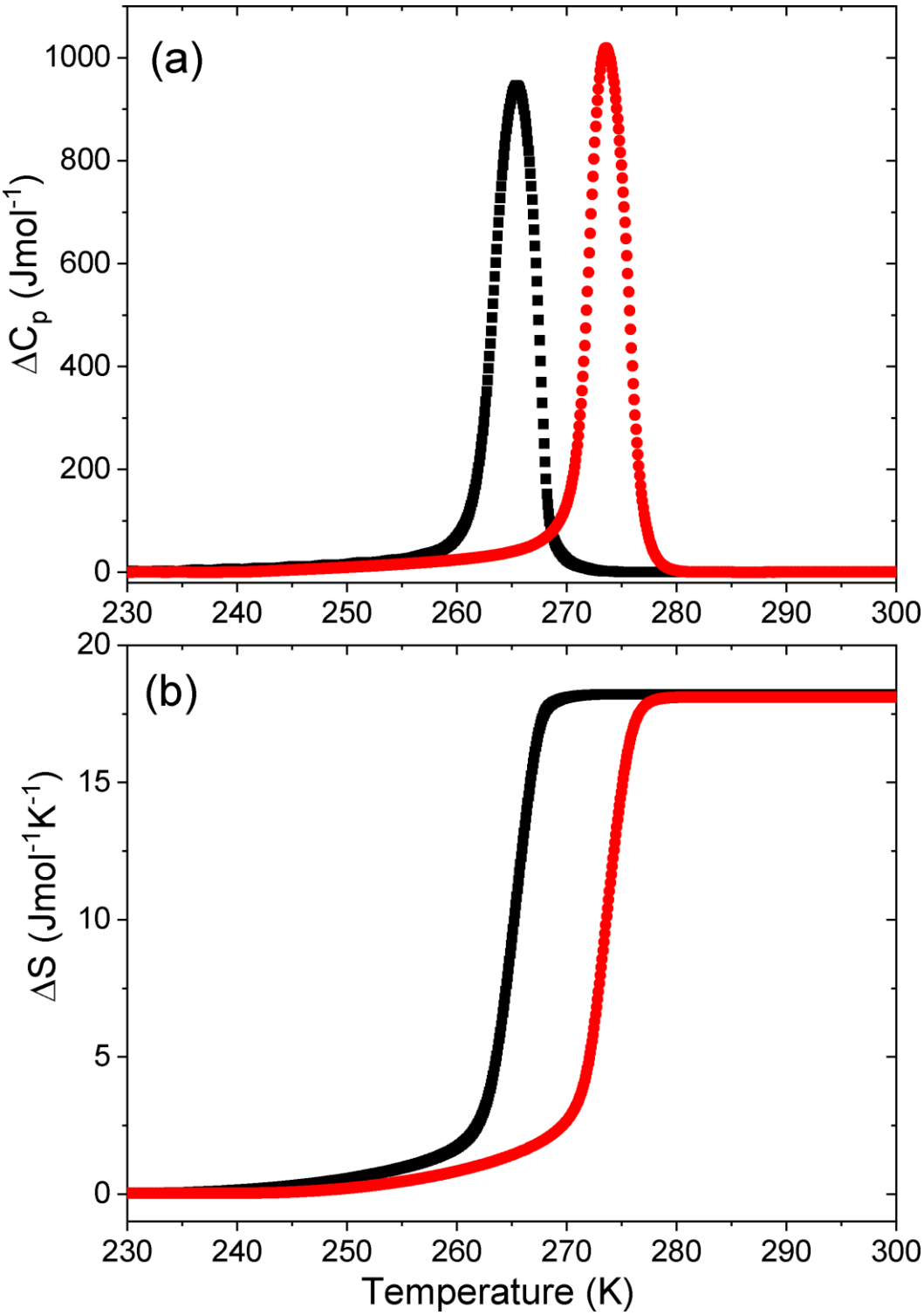

Figure S4. The change in C_p (a) and S (b) for BeTriMeCd in 2nd run: cooling is denoted by black line and heating by read line.

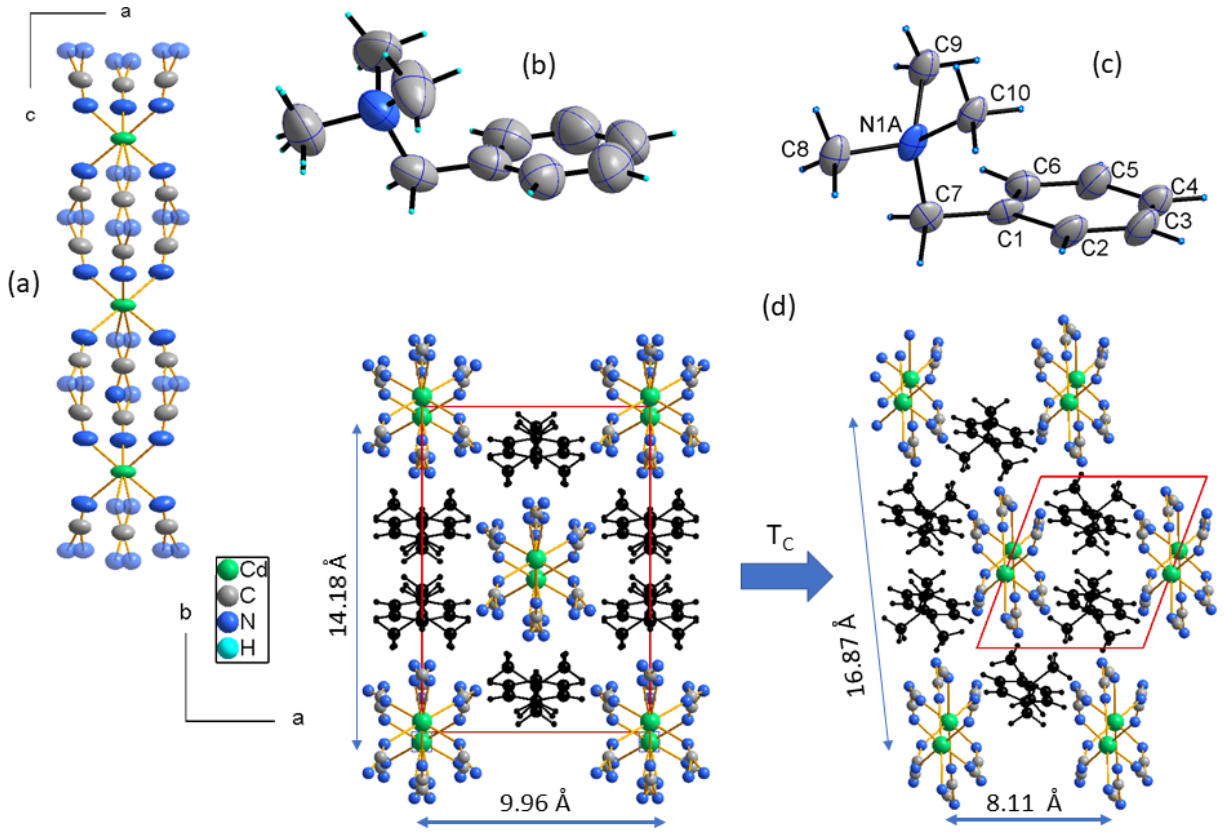

Figure S5. The details of the crystal structure of BeTriMeCd in (a)-(b) Phase **I**, (c) BeTriMe$^+$ in Phase **II** with atom numbering, the displacement ellipsoids are drawn at 50% probability, (d) distortion of the crystal structure as seen along the polar direction. In **II** radical elongation of the interchain distance in b_{ortho} occurs, on the other hand, the interchain distances in a_{ortho} are reduced in a comparable degree.

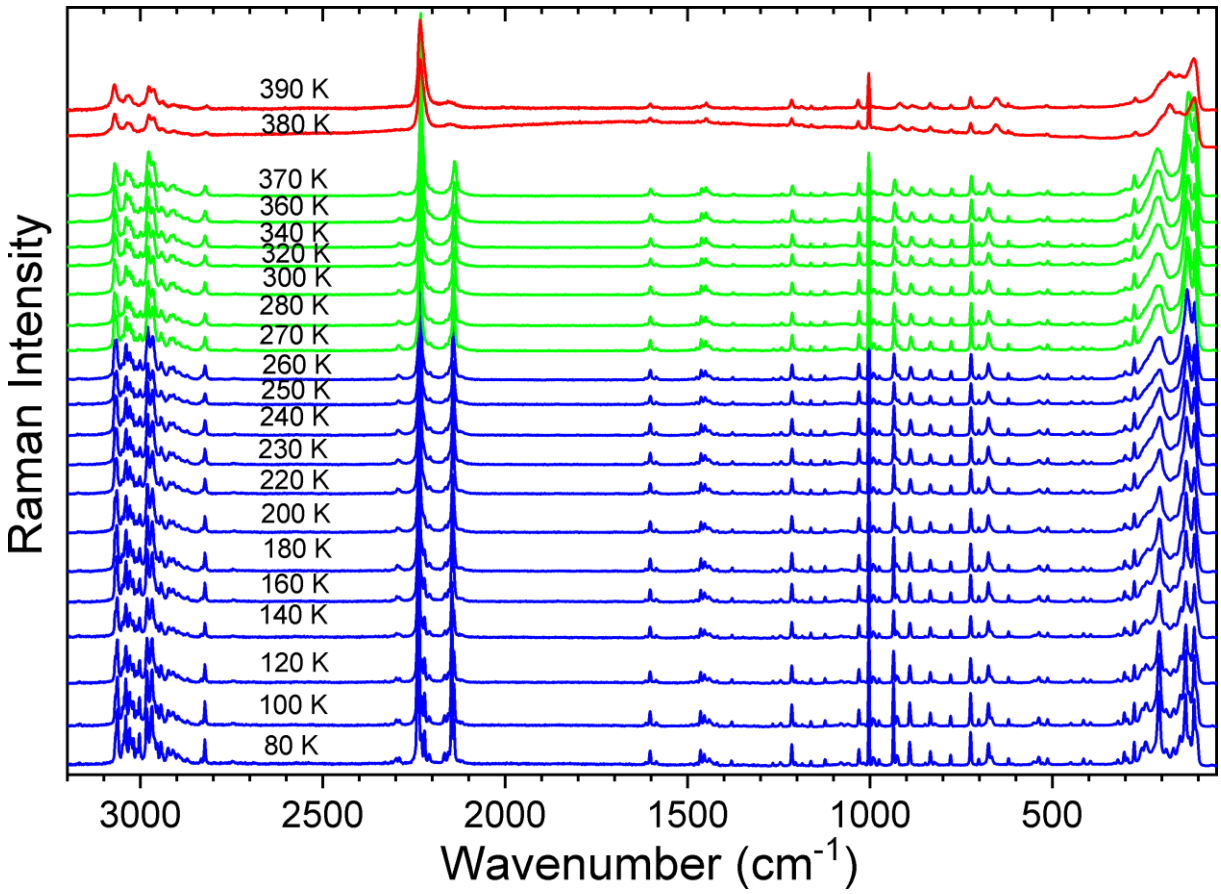

Figure S6. Raman spectra of BeTriMeCd in the heating run from 80 to 390 K (3200-50 cm^{-1} range).

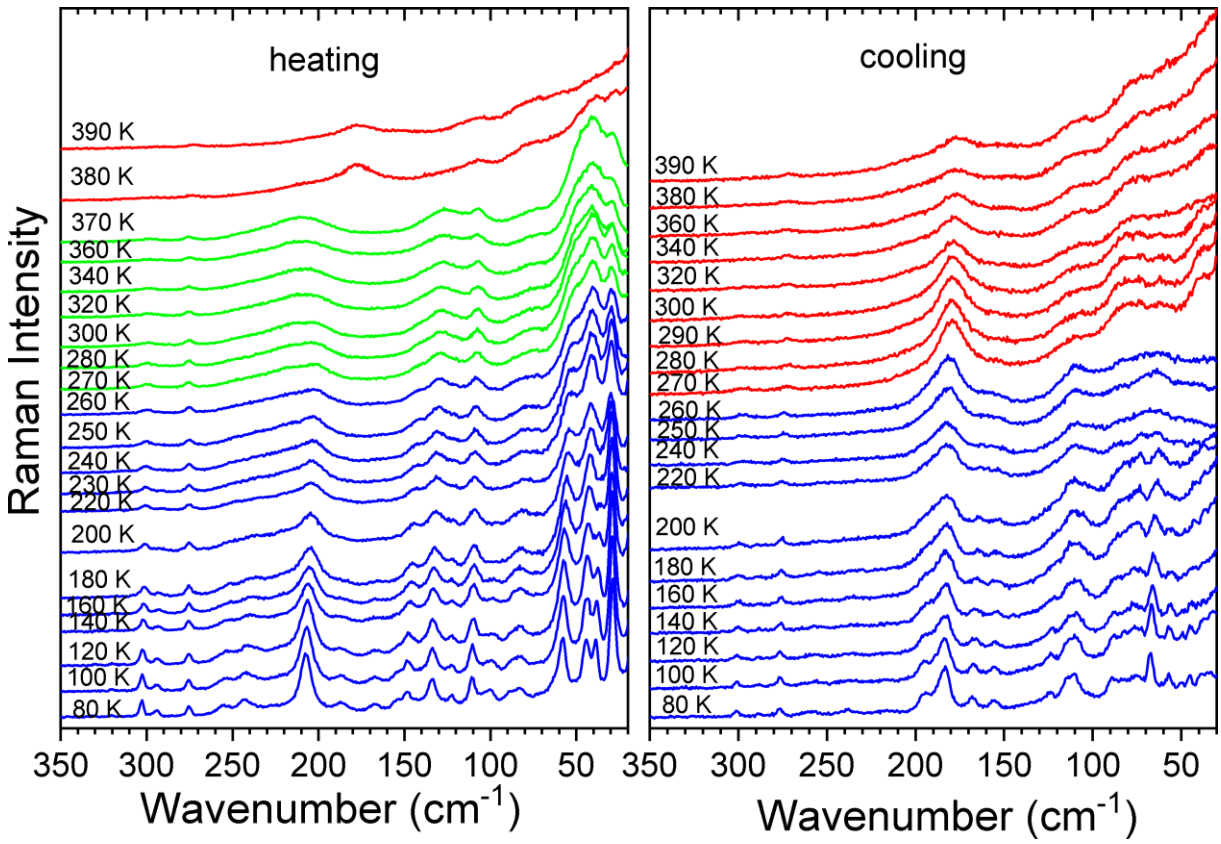

Figure S7. Low-wavenumber Raman spectra of BeTriMeCd measured using the Eclipse filter in the heating (left panel) and cooling (right panel) runs.

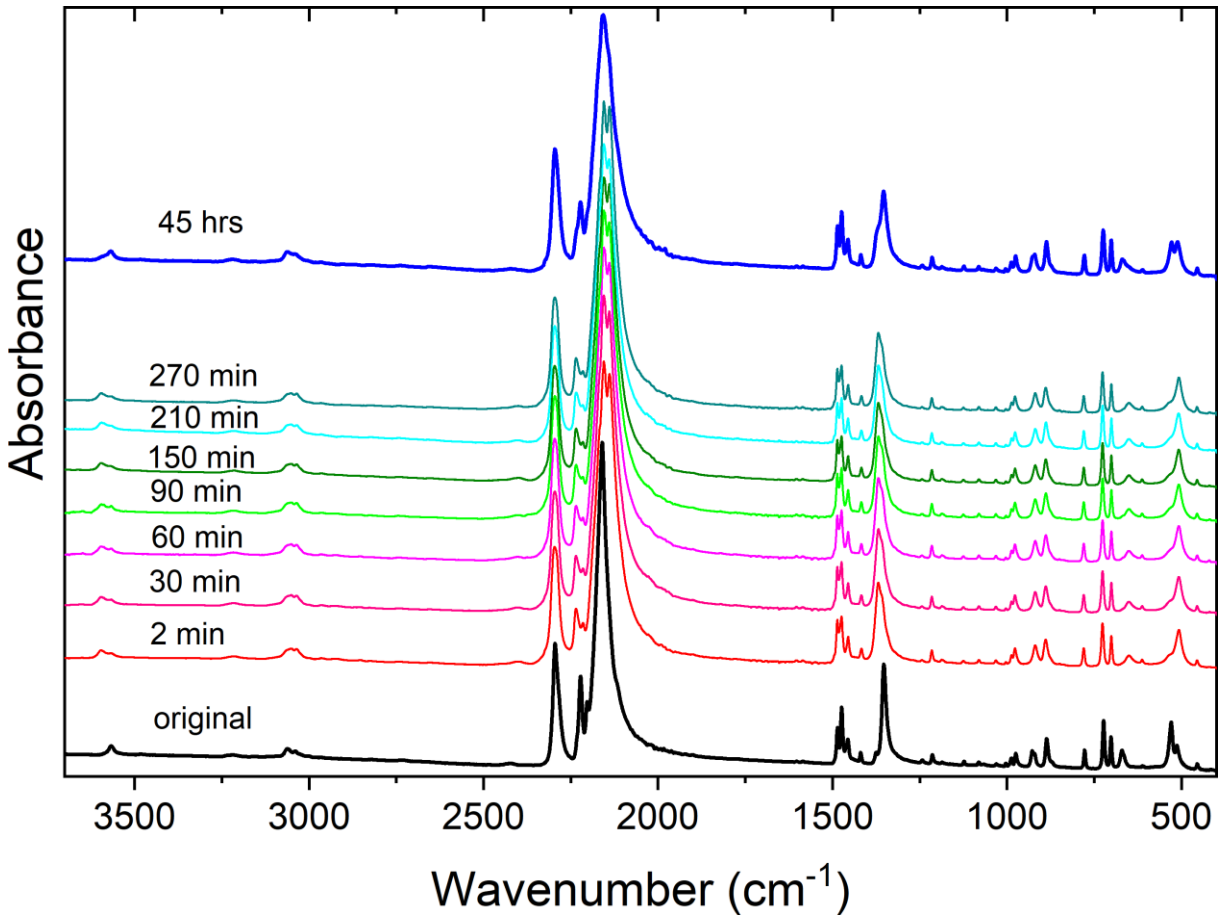

Figure S8. ATR spectra of the original BeTriMeCd sample and the same sample heat-treated at 400 K and kept at room-temperature for 2, 30, 60, 90, 150, 210 and 270 min as well as 45 hours.

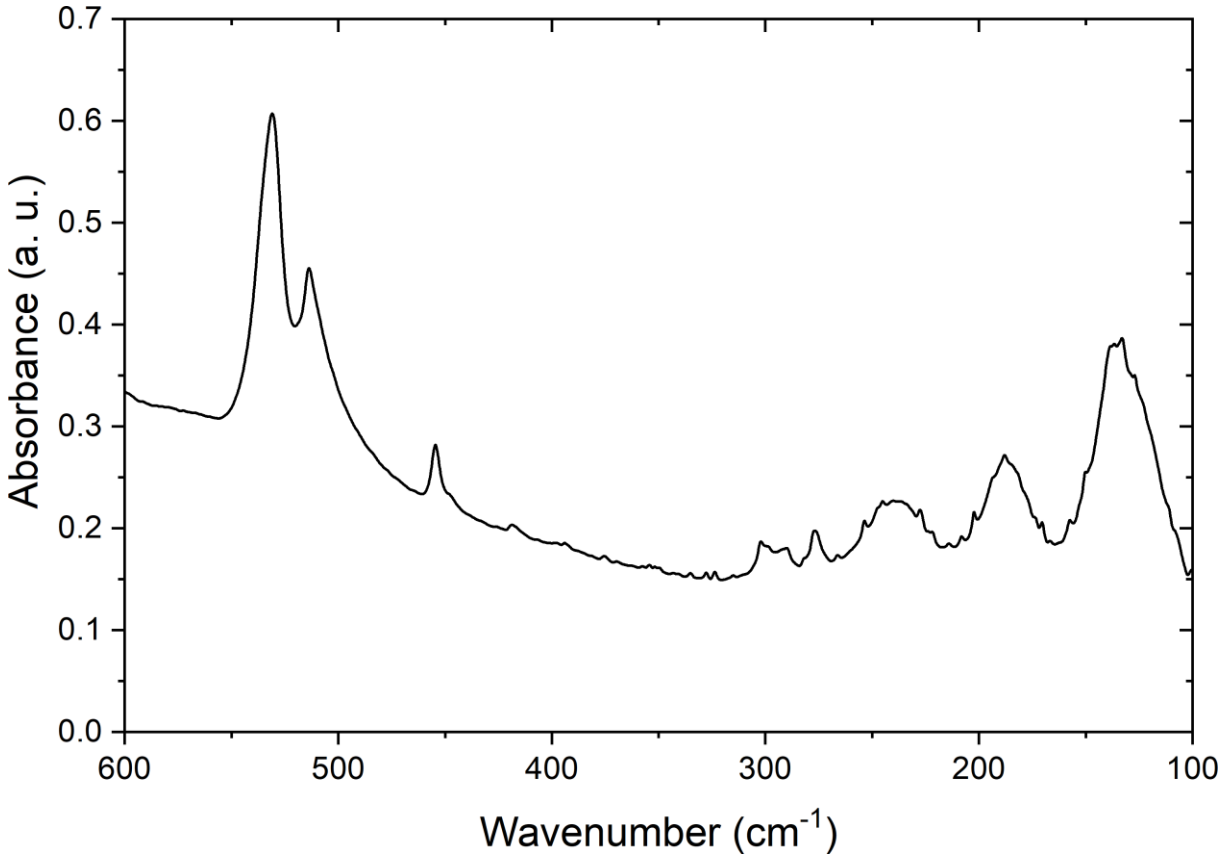

Figure S9. Far-IR spectrum of BeTriMeCd recorded at RT.

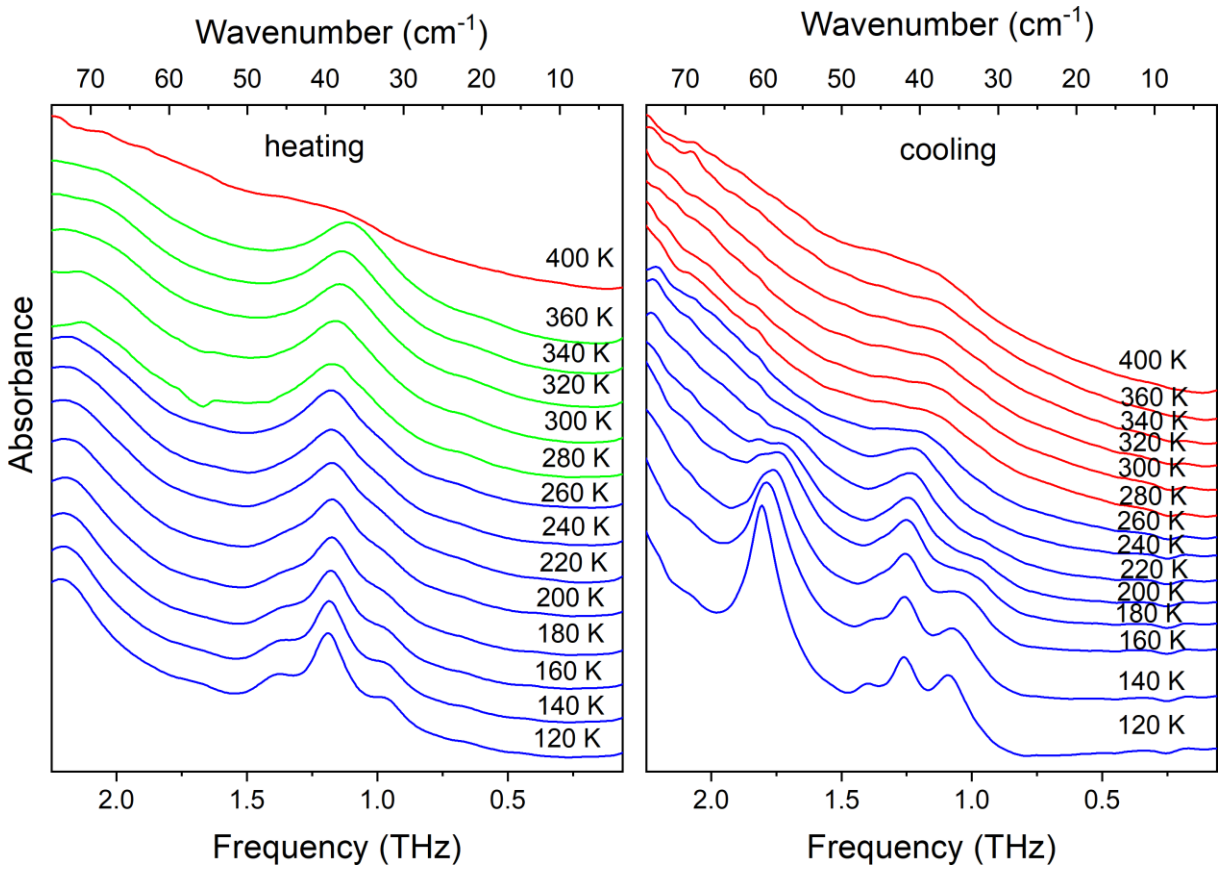

Figure S10. Temperature-dependent THz spectra of BeTriMeCd recorded in the heating and cooling runs.

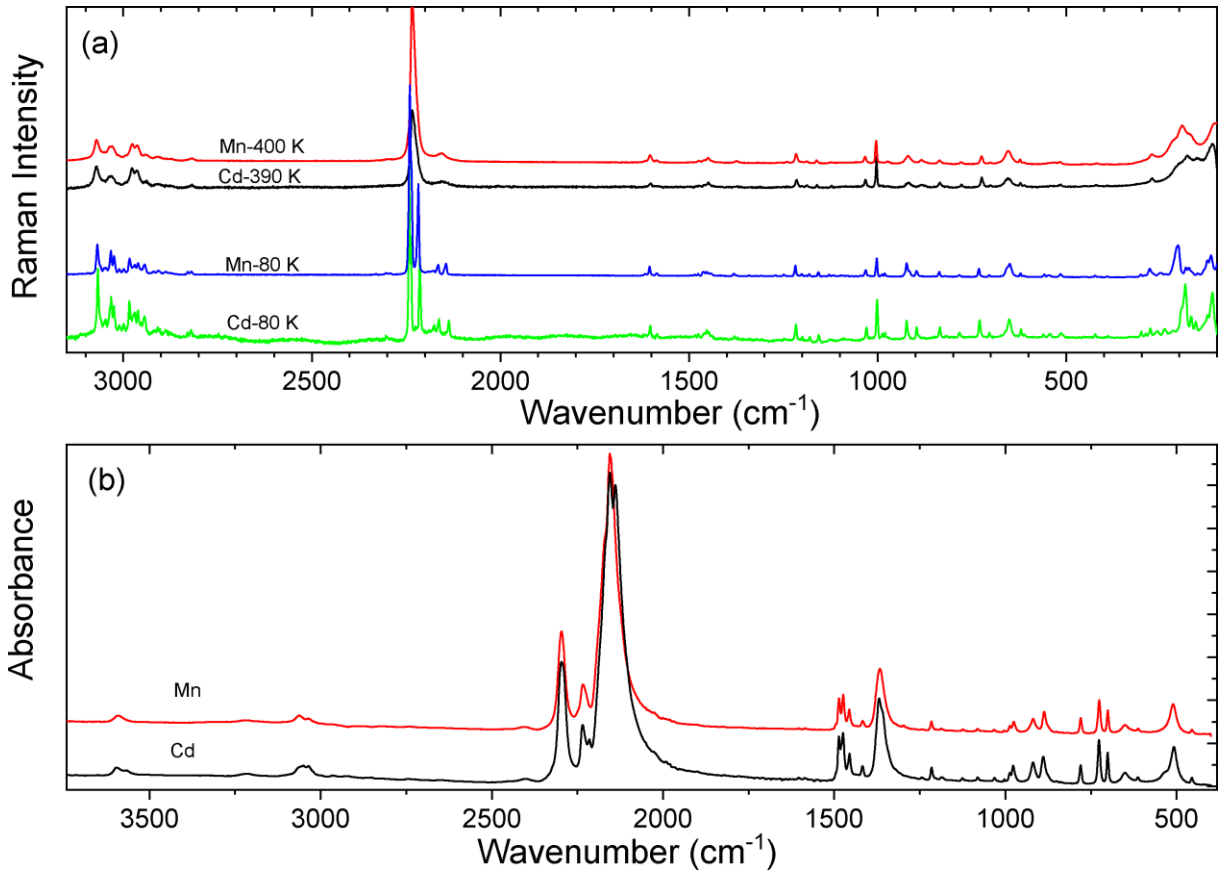

Figure S11. (a) Raman spectra of the BeTriMeCd and BeTriMeMn samples measured at 390 and 400 K, respectively, and the spectra of the same compounds recorded for the heat-treated samples at 80 K. (b) RT ATR IR spectra of the BeTriMeCd and BeTriMeMn samples heat-treated at 400K.

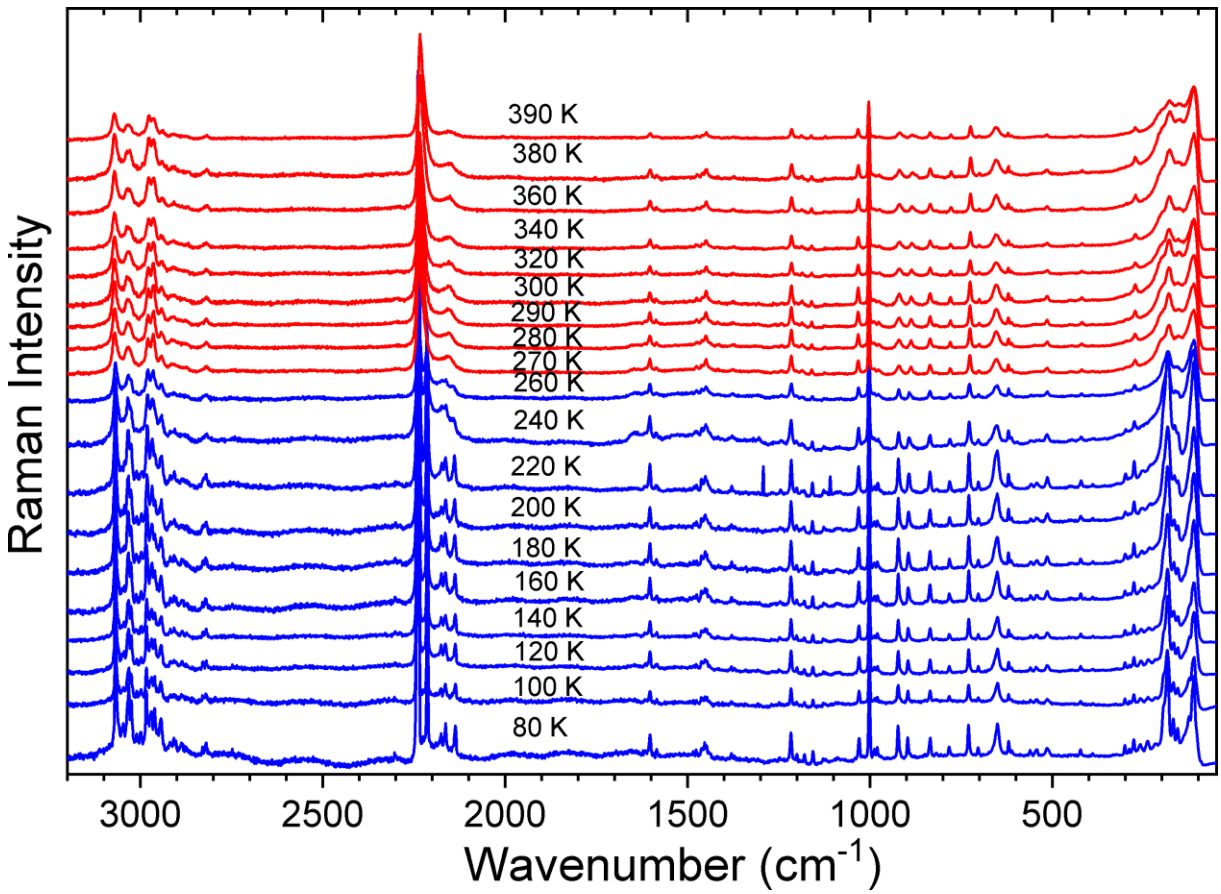

Figure S12. Raman spectra of BeTriMeCd in the cooling run from 390 to 80 K (3200-50 cm^{-1} range).

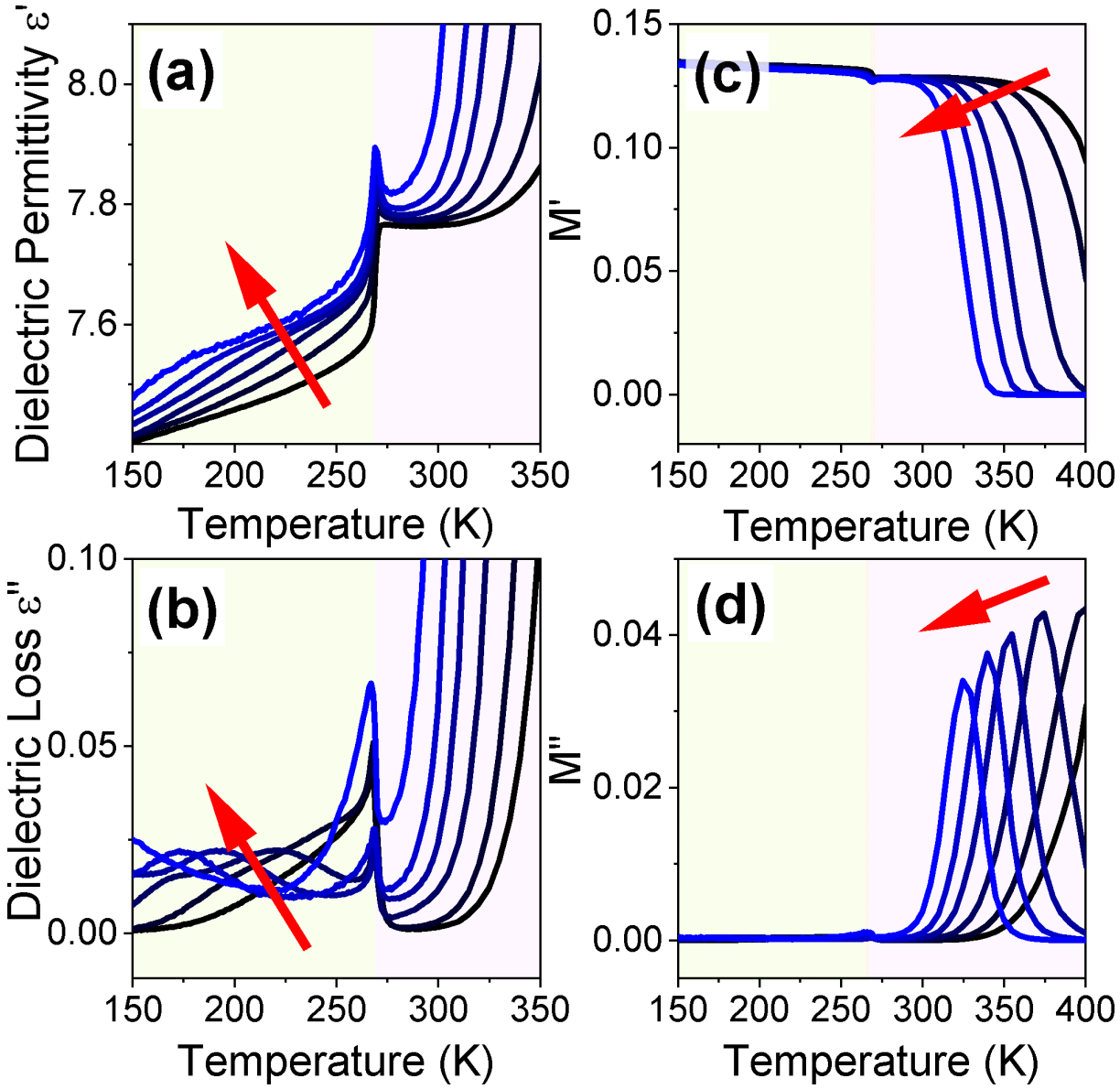

Figure S13. Temperature dependence of the complex dielectric permittivity ε' (a) dielectric loss ε", (b) and electric modulus parts M' (e), M" (f) for selected frequencies from the range 10Hz to 1MHz for BeTriMeCd polycrystalline sample. The marked areas indicate the different phases during cooling from 400K.

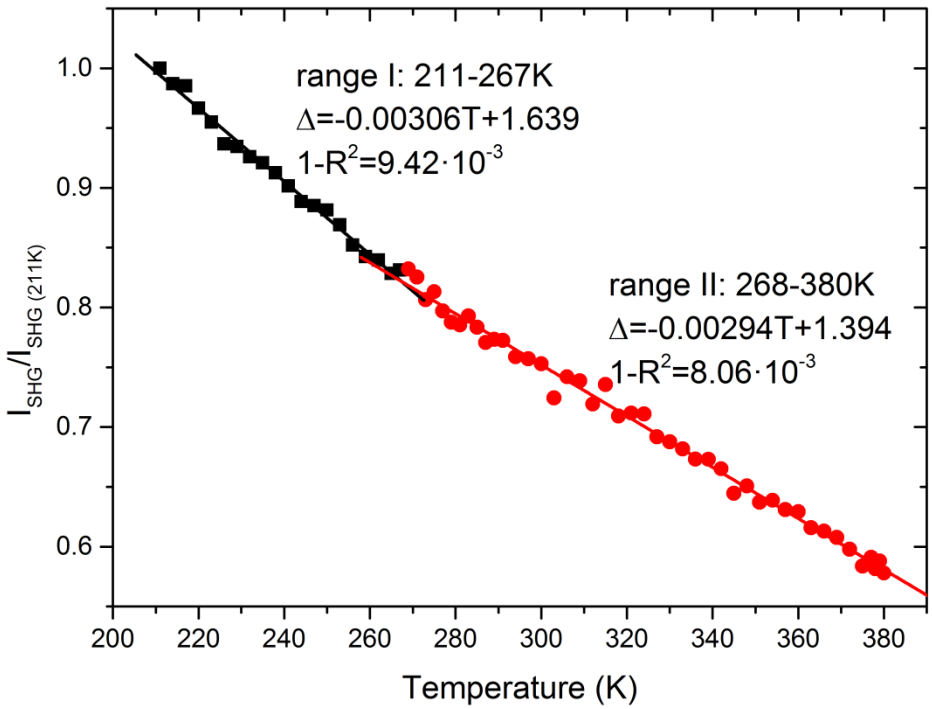

Figure S14. Plot of thermometric parameter Δ ($\Delta = I_{SHG}/I_{SHG}(211K)$) in the function of temperature for BeTriMeCd. Linear functions led through two sets of points serve as calibration curves.

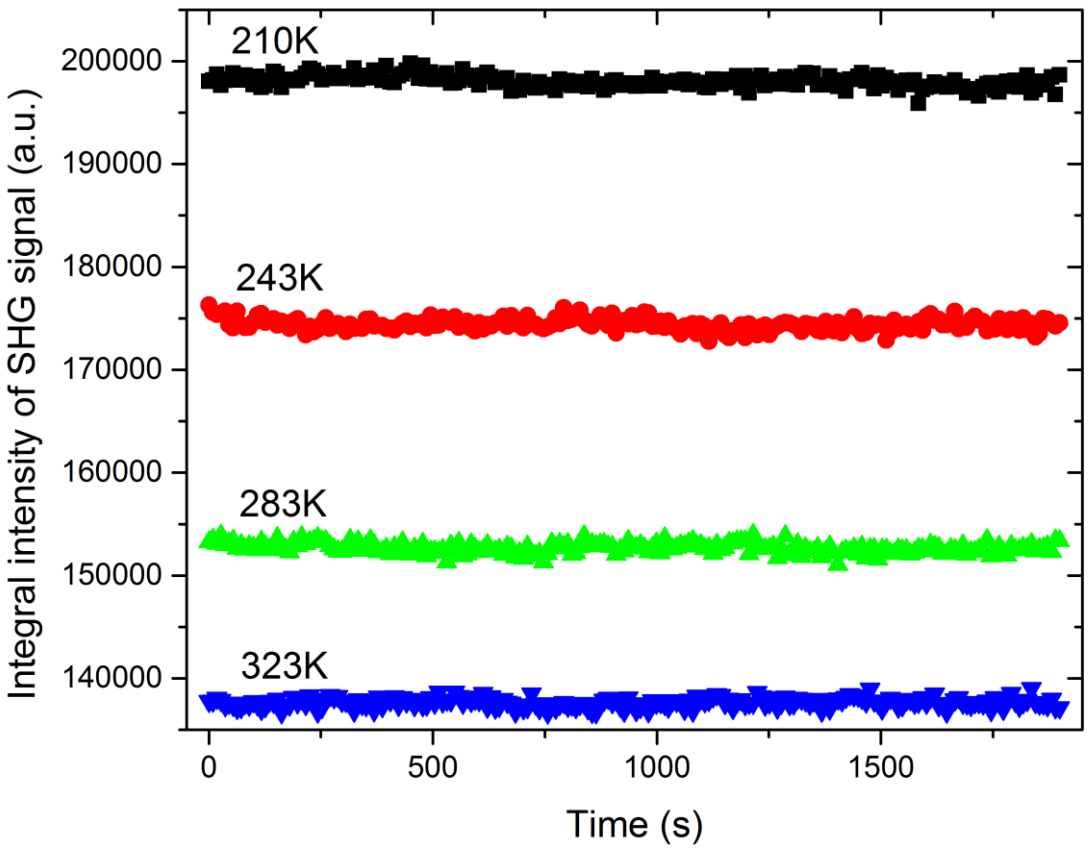

Figure S15. Stability plots of integral intensity of SHG signal in the function of irradiation time for BeTriMeCd registered for four temperature points: 210K, 243K, 283K, and 323K. Each set conisists of ca. 220 measurement points which were collected for a period of 30 minutes of laser irradiation. Data shown corresponds is not normalized vs. laser beam intensity, hence the signal ripple is due to minor fluctuation of fundamental beam provided by the femtosecond laser. It is apparent that BeTriMeCd is stable at each of these temperatures for at least 30 minutes of continuous laser irradiation. Laser beam parameters: 800 nm, 75 fs laser puleses at 1kHz repetition rate, 1.3 W/cm^2 power density.

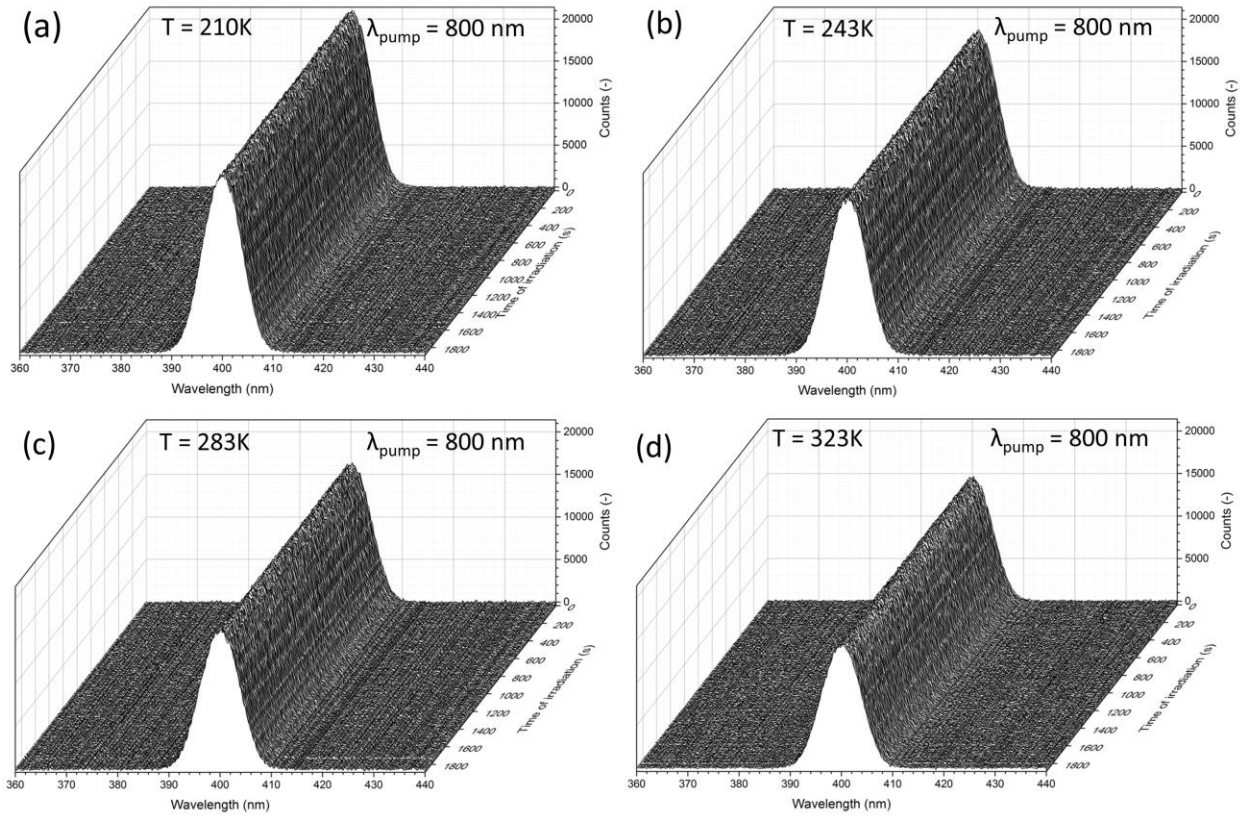

Figure S16. Experimental spectra collected during laser stability experiments at a) 210K, b) 243K, c) 283K, d) 323K.

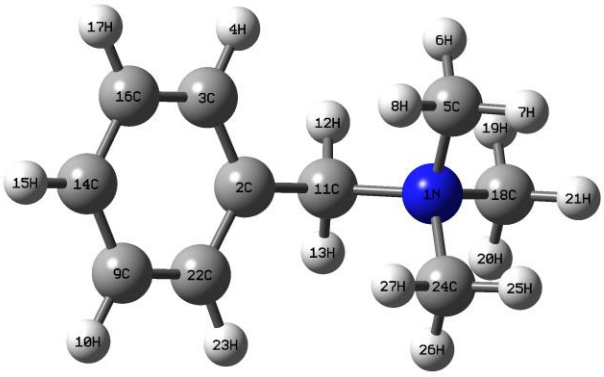

Figure S17. The structural model of the studied BeTriMe^{+} cation.

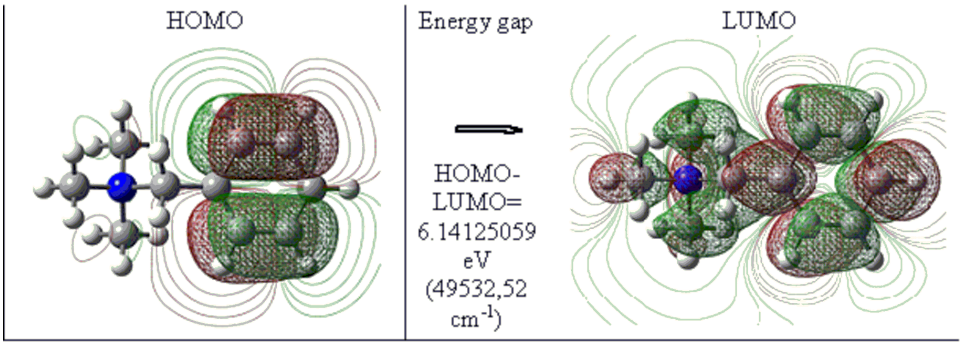

Figure S18. HOMO and LUMO orbitals and the HOMO-LUMO energy gap for the benzyltrimethylamine cation ($BeTriMe^+$). Detailed values: HOMO(41) = -0,38802 a.u., LUMO(42) = -0,16233 a.u., Energy gap = 0.22569 a.u. (6.14125059 eV, 49532,52 cm^{-1}).

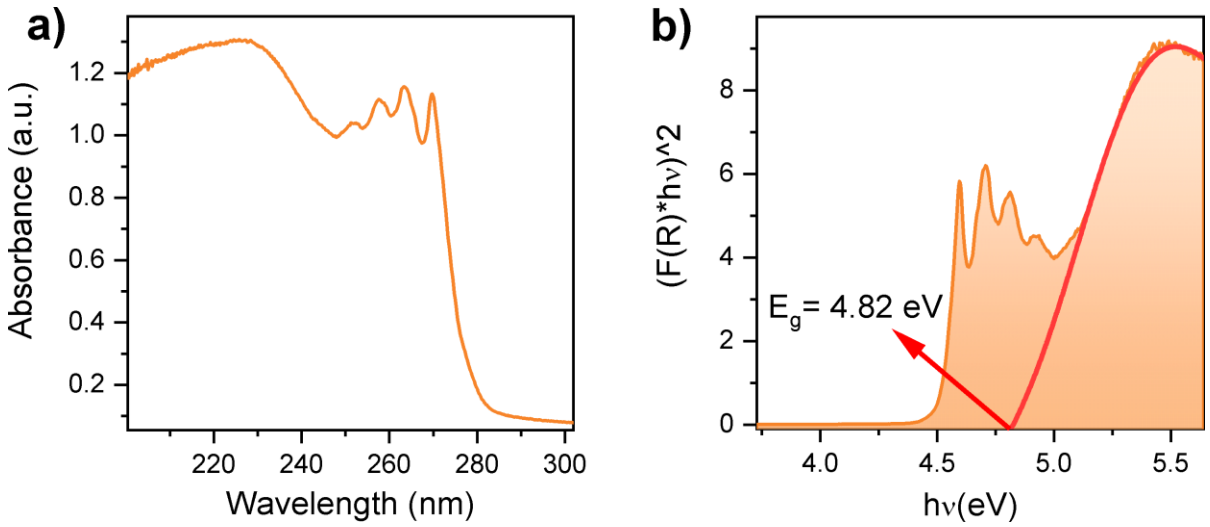

Figure S19. a) The absorbance spectra of BeTriMeCd and b) the energy band gap estimated using Kubelka–Munk function.